REPORT DOCUMENTATION PAGE

Form Approved
OMB No. 0705-0188

1. AGENCY USE ONLY (Leave blank)	2. REPORT DATE	3. REPORT TYPE AND DATES COVERED
	970228	Technical 3 Report, Dec '95-Nov '96

4. TITLE AND SUBTITLE

Synthesis of Ceramics from Solutions: Fuctionally Graded Composites,
NanoComposites and Single Crystal Thin Films

5. FUNDING NUMBERS

AFOSR
F49620-96-1-0003

6. AUTHOR(S)

Fred F. Lange

7. PERFORMING ORGANIZATION NAME(S) AND ADDRESS(ES)

Materials Department
College of Engineering
University of California
Santa Barbara, CA 93106-5050

8. PERFORMING ORGANIZATION REPORT NUMBER

9. SPONSORING/MONITORING AGENCY NAME(S) AND ADDRESS(ES)

Dr. Alexander Pechenik
AFOSR/PKA
110 Duncan Avenue, Suite B115
Bolling AFB DC 20332-8080

10. SPONSORING/MONITORING AGENCY REPORT NUMBER

11. SUPPLEMENTARY NOTES

12A. DISTRIBUTION/AVAILABILITY STATEMENT

A

12B. DISTRIBUTION CODE

13. ABSTRACT (Maximum 200 words)

Cubic perovskite films with different compositions were grown on perovskite substrates to investigate the influence of a large lattice mismatch on growth phenomena via the chemical solution deposition method, using toluene solutions of different 2-etyhlhexanoates and neodecanoates. The films were pyrolyzed to crystallize the perovskite of the desired composition and then heated to 1000°C to promote epitaxial grain growth. Pole figures obtained via X-ray diffraction as well as selected area diffraction (SAD) of TEM specimen with lattice mismatches of 2.5% ($SrTi_{0.5}Zr_{0.5}O_3$ on $SrTiO_3$), 5% ($SrZrO_3$ on $SrTiO_3$), 7.4% ($BaZrO_3$ on $SrTiO_3$) and 8.2% ($SrZrO_3$ on $LaAlO_3$) reveal only the epitaxial orientation [100](001) film || [100](001) substrate. The XRD and TEM results also indicate increasing polycrystallinity with increasing lattice mismatch. High resolution electron microscopy (HREM) of films on $SrTiO_3$ demonstrated that an array of misfit dislocations is present at the interface. The misfit dislocations have line vectors **l** of a<100>-type and Burgers-vectors **b** of a<010>-type. Dislocation separation distances obtained with HREM and XRD lattice parameter measurements show that the strain energy within the films, due to lattice mismatch, is nearly fully relaxed. The mechanisms of epitaxial growth and dislocation formation are discussed.

14. SUBJECT TERMS	15. NUMBER OF PAGES
Epitaxy, Perovskite, films, Mismatch Strain, $SrTiO_3$	48
	16. PRICE CODE

17. SECURITY CLASSIFICATION OF REPORT	18. SECURITY CLASSIFICATION OF THIS PAGE	19. SECURITY CLASSIFICATION OF ABSTRACT	20. LIMITATION OF ABSTRACT
Unclassified	Unclassified	Unclassified	

Synthesis of Ceramics From Solutions: Functionally Graded Composites, NanoComposites and Single Crystal Thin Films

Contract AFOSR F49620-96-1-0003

period: December 1995- November 1996

February 1997

From

Materials Department
College of Engineering
University of California
Santa Barbara, CA 93106

Technical Report 3

LATTICE MISMATCH ACCOMMODATION IN PEROVSKITE FILMS ON PEROVSKITE STRUCTURES

P.A. Langjahr, F.F. Lange, T. Wagner, and M. Rühle

In Press: Acta Met.

LATTICE MISMATCH ACCOMMODATION IN PEROVSKITE FILMS ON PEROVSKITE SUBSTRATES

P.A. Langjahr [1], F.F. Lange [2], T. Wagner [1], and M. Rühle [1]

[1] Max-Planck-Institut für Metallforschung, D-70174 Stuttgart, Germany and [2] Materials Department, University of California, Santa Barbara, CA 93106, USA

Abstract

Cubic perovskite films with different compositions were grown on perovskite substrates to investigate the influence of a large lattice mismatch on growth phenomena via the chemical solution deposition method, using toluene solutions of different 2-etyhlhexanoates and neodecanoates. The films were pyrolyzed to crystallize the perovskite of the desired composition and then heated to 1000°C to promote epitaxial grain growth. Pole figures obtained via x-ray diffraction as well as selected area diffraction (SAD) of TEM specimen with lattice mismatches of 2.5% ($SrTi_{0.5}Zr_{0.5}O_3$ on $SrTiO_3$), 5% ($SrZrO_3$ on $SrTiO_3$), 7.4% ($BaZrO_3$ on $SrTiO_3$) and 8.2% ($SrZrO_3$ on $LaAlO_3$) reveal only the epitaxial orientation [100](001) film || [100](001) substrate. The XRD and TEM results also indicate increasing polycrystallinity with increasing lattice mismatch. High resolution electron microscopy (HREM) of films on $SrTiO_3$ demonstrated that an array of misfit dislocations is present at the interface. The misfit dislocations have line vectors **l** of <100>-type and Burgers-vectors **b** of <010>-type. Dislocation separation distances obtained with HREM and XRD lattice parameter measurements show that the strain energy within the films, due to lattice mismatch, is nearly fully relaxed. The mechanisms of epitaxial growth and dislocation formation are discussed.

1. INTRODUCTION

A number of different methods are used to overgrow a thin, single crystal film of one material on a single crystal substrate of another material - a process known as epitaxy. The periodicity of the atoms on a substrate surface is the template for the epitaxial growth of the thin film material. Even when the two materials have the same structure, their periodicity is generally not identical, i.e., their lattice parameters are different ($d_f \neq d_s$). If the film grows coherently on the substrate, i.e., when the periodicity of the film exactly reproduces the periodicity of the substrate, the difference in lattice parameter gives rise to a residual strain as summarized by Sutton and Balluffi [1]. Because tractions within the film and substrate must sum to zero and the substrate is substantially thicker, all of the residual strain resides within the film (neglecting positions close to the edge of a finite film). The strain in directions parallel to the interface is either compressive or tensile, depending on whether d_f is either greater or smaller than d_s, respectively. This in-plane strain is given by

$$e_{||} = -\frac{d_f - d_s}{d_f} = -\varepsilon_s \frac{d_s}{d_f} \qquad (1)$$

(ε_s = lattice mismatch strain).

Coherent films are rarely observed unless the lattice mismatch is very small, or as discussed below, the film is extremely thin. Instead, it is well known [1] that a network of dislocations forms at or very near the interface to relax most of the strain produced by the lattice mismatch. The dislocations are the terminus of either extra or missing lattice planes within the film, depending on the sign of

the in-plane strain. The extra or missing planes allow the film to have its unconstrained lattice parameter at very short distances away from the interface. If the strain within the film is fully relaxed, the distance S between dislocations is given by [2]

$$S = \frac{b}{|e_{\|}|}, \tag{2}$$

where b is the magnitude of the Burgers vector of the dislocation in terms of the substrate lattice.

For the case where the mismatch is small ($\varepsilon_s < 0.01$), and the film grows layer by atomic layer as observed for epitaxy through the vapor phase [3,4], the dislocation network appears to form by the expansion of dislocation loops at the film surface to the interface. This explanation is consistent because the dislocation network is only observed when the film thickness exceeds a critcal value; coherent (dislocation free) interfaces are observed before the film grows to its critical thickness. A critical thickness exists because the work needed to expand the dislocation loops is drawn from the residual strain energy in the film, and for a given material system, the strain energy per unit area is proportional to the film thickness [1]. Much less is known about the formation of the dislocation network when either the mismatch strain is large, which increases the tendency that the film grows by island coalesence, [4] or when a polycrystalline film is converted to a single crystal by an epitaxial grain growth phenomenon (Miller et al. [5]) as for the current study.

Systematic studies of either the epitaxy phenomenon or the accommodating dislocation network have not been reported for the case where ε_s exceeds ≈ 0.02. One problem in such a study is that the mismatch strain produced by the epitaxy

of a solid-solution composition, where the lattice parameter of the film can be systematically changed relative to the substrate, rarely exceeds 0.02 [5]. Interdiffusion of the film material into the substrate, which would produce a film with a 'graded' lattice parameter, is a second problem.

Both problems could be overcome using double oxide compositions with the perovskite structure that include $SrZrO_3$, $BaZrO_3$ and $BaCeO_3$ and their solid-solutions (e.g., $SrTi_{0.5}Zr_{0.5}O_3$ and $BaCe_{0.5}Zr_{0.5}O_3$) that epitaxy on commercially available perovskite substrates, $SrTiO_3$ and $LaAlO_3$. This compositional series of identical structures allows a systematic study of lattice mismatches up to strains of 0.16.[a] Initial work showed that these compositions could be grown epitaxially without interdiffusion at temperatures up to 1100°C. Results of interdiffusion studies at higher temperatures will be published in a subsequent paper [7].

Perovskite films are widely investigated for dielectric and opto-electric device applications that include ceramic capacitors ($SrTiO_3$, $SrZrO_3$ and their solid solutions [8] and $BaZrO_3$ [9]). $BaZrO_3$ and $SrTiO_3$ are cubic at room temperature, whereas the other compositions are only cubic at high temperatures (Taylor [10]). They undergo cubic to pseudo-cubic phase transformations during cooling. Since deviations from cubic symmetry are small (shear strains < 0.003) compared to the lattice mismatch (between 0.025 and 0.16), we neglect these transformation and use the pseudocubic lattice constants in this study. For example, the orthorhombic lattice parameters of $SrZrO_3$ [11] have been transformed to a mean pseudocubic lattice parameter as described by Taylor. For the $LaAlO_3$ substrate, which is rhombohedral at room temperature, the pseudocubic lattice parameter is used from Geller and Bala [12].

[a] To the knowledge of the authors, except for sputter-grown $BaZrO_3$ on $SrTiO_3$ (Y. Dansheng et al. [6]), none of the interfaces studied here have been investigated before.

The inorganic, single crystal films were produced by the chemical solution deposition method, where a solution of different metalorganic compounds is used as a vehicle to deposit, by spin-coating, the desired elements on a single crystal substrate. During spinning, a precursor film forms, which is decomposed (pyrolyzed) to a polycrystalline film by heating at relatively low temperatures (< 400°C). The polycrystalline film is then converted into a single crystal film at higher temperatures by one of a number of mechanisms reviewed elsewhere [13]. One advantage of the chemical solution deposition method is its high degree of compositional control, inherent with other solution synthesis routes for multi-element, inorganic materials.

Preliminary observations of $SrZrO_3$ epitaxial films on $SrTiO_3$ showed a continuous film with periodic dislocations at the interface to accommodate lattice mismatch [14]. Here we report the detailed characterization of the films using x-ray diffraction (XRD), scanning electron microscopy (SEM), conventional transmission electron microscopy (TEM) and high resolution electron microscopy (HREM). The evolution of the precursor material is characterized by thermogravimetric analysis (TGA) and XRD. The separation distance between dislocations located at the interface was determined with HREM and correlated to lattice mismatch. Finally, the mechanisms of the epitaxial growth phenomena and the generation of the dislocation network are discussed.

2. EXPERIMENTAL PROCEDURE

Thin films of $SrTi_{0.5}Zr_{0.5}O_3$ on $SrTiO_3$, $SrZrO_3$ on $SrTiO_3$, $BaZrO_3$ on $SrTiO_3$ and $SrZrO_3$ on $LaAlO_3$ were prepared by spin-coating (001)-oriented, polished $SrTiO_3$ (Coating & Crystal Technology, Kittanning, PA, USA) and $LaAlO_3$

substrates with metalorganic precursor solutions. The cubic and pseudocubic lattice parameters of these systems and their room temperature mismatch strains are listed in Table 1.

Prior to spin-coating, the substrates were cleaned with tri-chloro-ethane, acetone and iso-propanol and heated for 2h at 1400°C to remove contamination and plastic deformation produced by polishing. The surface of the $SrTiO_3$-substrate shows steps, probably due to a miscut as shown in Fig. 1.

Precursors of Ce- and Zr-2-ethylhexanoates, Ba- and Sr-neodecanoates and Ti-2-ethylhexoxide (STREM Chemicals, Newburyport, MA, USA) were used. The Ti-precursor was solubilized in toluene under nitrogen, as recommended by Polli et al. [15], which reduces the hygroscopic nature of the Ti-precursor. Precursor solutions, previously assayed for their oxide content were mixed to achieve the appropriate composition and then diluted with toluene prior to spin-coating, such that the molarity of the final precursor solution was ≈ 0.25M. After mixing, the solutions were stirred for at least 15 minutes to ensure good mixing of the different precursor molecules on a molecular level. In order to remove precipitates that can lead to inhomogeneous films during spin-coating, the solutions were filtered (pore size in filter: 0.2μm). The decomposition of the precursors during heat treatment was investigated by TGA (General 4.1C, Du Pont 2000) using a heating rate of 10°C/min. The powder obtained during heat treatment was characterized by XRD (XDS2000, Scintag Inc., Sunnyvale, CA, USA). For the determination of the lattice constants, silicon was added as an internal standard.

The substrates were coated with two drops of precursor solution, spin-coating after each drop for 10s with 4000 rpm. In order to pyrolyze the precursor and

initiate epitaxial growth, the films were heated up to 1000°C at a heating rate of 10°C/min in an air furnace for 1h.

The film morphology and structure was determined with XRD, x-ray pole figure analysis (MRD, Philips, Eindhoven, The Netherlands), SEM (JEOL6300FE) and TEM (JEOL2000FX operated at 200kV). The investigation of the structure at the interface was performed with HREM (JEOL4000EX operated at 400kV). TEM cross-section specimen were prepared as described by Strecker et al. [16].

3. RESULTS

3.1 Thermogravimetric analysis of powders

Figure 2 shows the TGA of the $SrZrO_3$- and $BaZrO_3$-precursors, results that are typical of the other mixed precursors. During heating, a large weight loss is observed due to the evaporation of solvent and the pyrolysis of the metalorganic precursors to an inorganic powder. The decomposition temperature, above which weight changes were negligible, was 372°C for $SrZrO_3$ and 361°C for $BaZrO_3$.

3.2 X-ray diffraction of powders

Figure 3 shows XRD powder spectra for precursors heated at 1000°C/1h. In the case of $SrTi_{0.5}Zr_{0.5}O_3$, the reflections are broadened and show shoulders on both sides, indicating, that $SrZrO_3$ and $SrTiO_3$ are not completely mixed. In the case of $SrZrO_3$ and $BaZrO_3$, single phase perovskite material was obtained as indicative of the sharp diffraction peaks. Lattice constants, d_p, listed in Table 2, were determined from the diffraction angles 2θ of the (002) reflections of the powder by using Bragg's equation (λ = 0.1541838nm) using the Si internal standard. They

agree well with literature values (Table 1). Scherrer's formula [17] was used to estimate the crystallite size in the $SrZrO_3$ and $BaZrO_3$ powder from the full width at half-maximum (fwhm) B of the (002) reflections. Instrumental broadening, B*, was determined from the fwhm of the (002) reflection of a $SrTiO_3$ single crystal substrate (that should show no size effect) as $B^* \approx 0.09°$. Instrumental broadening B* was subtracted from the total fwhm, B, using the simplified approach described by Warren and Biscoe [18], which assumes that the x-ray diffraction peak has the shape of an error function. Using the values obtained for $SrZrO_3$ and $BaZrO_3$ powders, $B \approx 0.4°$, the grain size was estimated as $D_p \approx 22$ nm.

3.3 X-ray diffraction of thin films

The crystallographic orientation of the films was determined by (θ-2θ) x-ray scans. Figure 4 shows measurements for $SrTi_{0.5}Zr_{0.5}O_3$, $SrZrO_3$ and $BaZrO_3$ on $SrTiO_3$ (mismatch: 2.5%, 5% and 7.4%). Figure 5 shows the result for $SrZrO_3$ on $LaAlO_3$ (8.2%). In all cases, the only film orientation was $(001)_f \,||\, (001)_s$, detected by intense (002) reflections in the x-ray spectra. Additional peaks in Figs. 4 and 5 are due to the substrate (002) reflection of the wavelength $CuK\alpha$ and others in the x-ray source ($CuK\beta$, $WL\alpha 1$ and $WL\alpha 2$). Theoretical values of 2θ of the (002) reflections of the substrates calculated by Bragg's equation were used for calibration. Lattice constants perpendicular to the interface, $d_\perp$, determined from the $(002)_f$ reflections, are listed in Table 3. For $SrZrO_3$ on $LaAlO_3$, the values of the lattice constants of film and powder agree very well, whereas in the case of the films on $SrTiO_3$, the film constants are slightly smaller than the powder constants. A peak shift may either result from residual stresses within the film (for example due to a thermal expansion mismatch, phase transformations or defects) or interdiffusion or a combination of both. Further experiments on $SrZrO_3$- and $BaZrO_3$-films on $SrTiO_3$ showed, that interdiffusion becomes

significant only above 1150°C [7]. No change in lattice constant was observed for heat treatments between 600°C and 1000°C.

As in the case of the powders, a rough estimation of the average grain size D_f for the grains within the film is calculated from the full width at half-maximum (fwhm) B of the (002) film reflections by applying Scherrer's and Warren's formulas. The values for B and D_f are listed in Table 3. The broadening that is included in the Scherrer formula is due to a reduced coherence length through a limited extension of the crystal normal to the reflecting planes. The estimated size of the (001)-oriented 'mosaic' grains normal to the substrate for the $SrZrO_3$ and $BaZrO_3$ films heat treated at 1000°C/h is in the range 30-40nm. The grains therefore are larger in the films than in the powders (see section 3.2). This indicates, that epitaxial grain growth in the films is enhanced compared to grain growth in powders. The larger full width at half-maximum in the case of $SrTi_{0.5}Zr_{0.5}O_3$ may be attributed to uncomplete mixing as the case for the powder.

Rocking-curves of the (002) film reflections show, in all cases, a very narrow full width at half-maximum ($\alpha \approx 0.5°$), indicating that the lattice planes of the films are oriented parallel to the substrate. The same fwhm ($\alpha = 0.4°$ to $0.5°$) is obtained for the substrates themselves [(002) $SrTiO_3$- and (002) $LaAlO_3$-reflections], suggesting that the out-of-plane orientation of the film is as good as the one of the substrates, regardless of lattice mismatch, within the error of measurement.

The in-plane orientation has been determined by pole figure analysis of three reflections: (002) film, (110) film and (110) substrate as shown by the example for $SrZrO_3$ on $SrTiO_3$ in Fig. 6. The (002) $SrZrO_3$ pole figure only shows a central diffraction peak, i.e. for a tilting angle of $\Psi \approx 0°$ [Fig. 6a)]. On the other hand, the

(110) pole figures [Fig. 6 b) and c)] show four reflections at identical positions at a tilting angle of $\Psi \approx 45°$ and four rotation angles Φ, that differ by 90°. These reflections are due to equivalent (110)-planes of (001)-oriented single crystals that satisfy the Bragg condition. Therefore, pole figure results show that the films have the same orientation as the substrate: [100](001) $SrZrO_3$ || [100](001) $SrTiO_3$. The same result is obtained for the other materials ($SrTi_{0.5}Zr_{0.5}O_3$ on $SrTiO_3$, $BaZrO_3$ on $SrTiO_3$ and $SrZrO_3$ on $LaAlO_3$). However, it should be noted, that in the case of the latter ones, there is an increased background in the center of the (110) $BaZrO_3$ - and (110) $SrZrO_3$ - pole figure (Fig. 7), indicating an increasing amount of polycrystallinity with increasing lattice mismatch.

3.4 SEM and conventional TEM results

Fig. 8 shows an SEM-micrograph of a $SrZrO_3$ film on $SrTiO_3$. As can be seen, relatively smooth films can be obtained. The films of $SrTi_{0.5}Zr_{0.5}O_3$ and $BaZrO_3$ are not perfectly homogeneous. In Figure 9 an SEM-micrograph of a $SrZrO_3$-film on $LaAlO_3$ is presented. The film is not continuous, but consists of a network of connecting islands.

As an example, a cross-sectional TEM-micrograph of a $SrZrO_3$ film on $SrTiO_3$ is shown in Fig. 10. The thickness of all films investigated by TEM, ≈ 25-50nm, is consistent with the coherence length, D_f, estimated from XRD. Porosity is observed in some portions of the films, which partially may have been introduced during ion-milling. Selected area diffraction (SAD) of TEM cross-sections of $SrTi_{0.5}Zr_{0.5}O_3$, $SrZrO_3$ and $BaZrO_3$ films confirms the epitaxial orientation relationship [100](001)$_f$ || [100](001)$_s$. The same is observed for $SrZrO_3$ on $LaAlO_3$. SAD of different regions also indicates, that some grains in films of $BaZrO_3$ on $SrTiO_3$ and $SrZrO_3$ on $LaAlO_3$, i.e., those with higher mismatch, do

not have the same orientation as the substrate. These results are consistent with XRD observations of these films, namely the increase of polycrystallinity with increased lattice mismatch.

3.5 HREM results

In order to determine the nature of the dislocation network, interfaces were imaged by HREM along two different zone-axes. Figure 11 shows HREM images of a $SrZrO_3$ film on $SrTiO_3$ heat treated at 900°C/1h in a) <100> and b) <1$\bar{1}$0> zone axis directions. A semicoherent interface with misfit dislocations is observed. As the lattice constant is larger for the film than for the substrate, the extra half-planes are located within the substrate, as expected. In both images, Burgers-circuits can be traced leading to closure failures of $\mathbf{b} = d_s$ <010> for imaging along the <100> zone axis and $\mathbf{b} = d_s/2$ <110> for the other case. In the latter case, the distance between the disturbed regions is approximately a factor of $\sqrt{2}$ smaller than in the first. The two different cases appear to be contradictory, as only one type of dislocation network should be present. However, this apparent conflict only reflects the fact that a lattice mismatch at the interface is present in both different zone axes. This is demonstrated schematically in Fig. 12 in a geometrical model for simple cubic lattices (O-lattice, Bollmann [19]). As can be seen, the closure failures and their distances observed can be explained purely geometrical. From the O-lattice model, a dislocation network with line-vectors $\mathbf{l} = d_s$ <100> and Burgers-vectors $\mathbf{b} = d_s$ <010> would be expected. The occurence of a relaxation of this type has been demonstrated by an analysis of the structure and the strain field from quantitative HREM-investigations [20]. Results from Z-contrast imaging are consistent with the results from HREM-investigations [21]. Figure 13 shows lower magnification HREM micrographs of a) $SrTi_{0.5}Zr_{0.5}O_3$, b) $SrZrO_3$ and c) $BaZrO_3$ on $SrTiO_3$ along the <100> zone showing that the separation

between dislocations decreases with increasing lattice mismatch. The distances between dislocations were determined on a microscopic level by counting atomic planes within the film and the substrate in <010>-direction; these are listed in Table 4 (S_{HREM}). The variability of the dislocation spacing is very high in the case of $SrTi_{0.5}Zr_{0.5}O_3$ on $SrTiO_3$, due, it appears, to compositional variations within these films, as suggested by XRD observations. Figure 13 also indicates that the dislocation cores always are located within the film material, either directly at or close to the interface. Dislocations within the bulk film material were occasionally observed. Values of the dislocation distances expected for fully relaxed films are estimated from x-ray powder lattice constants d_p with equations (1) and (2) ($d_f = d_p$ and $b = d_s \approx 0.3905$nm), see Table 4 (S_p). The separation distances observed in HREM-micrographs are in good agreement with those calculated from x-ray powder data, showing that the lattice mismatch is basically accommodated by misfit dislocations.

4. DISCUSSION

4.1 Epitaxial growth

Apart from small amounts of polycrystallinity for the higher mismatched systems $BaZrO_3$ on $SrTiO_3$ and $SrZrO_3$ on $LaAlO_3$ (see Fig. 7), the perovskite films were epitaxial. These observations suggest that epitaxy takes place by a mechanism described by Miller et al. [5] for the case of cubic $Zr(Y)O_2$ on $Zr(Y)O_2$. Epitaxy starts by heterogeneous nucleation of film grains at the interface and continues by the consumption of non-epitaxial grains. The driving potential is the elimination of grain boundaries.

4.2 Accommodation of lattice mismatch

The orientation of the dislocation network observed at the interface between the cubic and pseudocubic perovskites is consistent with observations by S. Stemmer et al. [22] in a similar system with perovskite structure ($PbTiO_3$ on $SrTiO_3$) grown by Pulsed Laser Deposition at 600°C. Because $\mathbf{b} = d\langle 010\rangle$ is the shortest complete translation vector of the perovskite structure, a dislocation with this Burgers vector would have the lowest line energy compared to other complete dislocations. Partial dislocations, on the other hand, with a shorter Burgers vector, e.g., $\mathbf{b} = d/2\ \langle 110\rangle$, as observed in PZT-ceramics [23], would have a lower line energy; however, an antiphase arrangement would be created at the interface that is not observed in the current work.

Apart from a slightly smaller film parameter $d_\perp$ than expected, suggesting, that the film is under a residual biaxial tension, the lattice mismatch is fully relaxed by periodic misfit dislocations for the cases of $SrTi_{0.5}Zr_{0.5}O_3$, $SrZrO_3$ and $BaZrO_3$ films on $SrTiO_3$. Because of the cubic to tetragonal phase transformation of $PbTiO_3$ during cooling, this was not observed for $PbTiO_3$ on $SrTiO_3$ [22]. A further difference between the two studies concerns the location of the dislocations relative to the interface. In the current study, the dislocations are located at or close to the interface in the $SrTi_{0.5}Zr_{0.5}O_3$, $SrZrO_3$ and $BaZrO_3$ films on $SrTiO_3$. In the $PbTiO_3/SrTiO_3$ study, no dislocations could be found directly at the interface; instead, the dislocations in $PbTiO_3$ exhibit a stand-off of a few nm from the interface. According to Mader and Knauss [24], a stand-off can be caused by the balance between image forces due to the difference in elastic properties of films and substrate and coherency forces on the dislocation. The fact that the equilibrium distance for the stand-off calculated by Mader and Knauss is inversely proportional to the lattice mismatch would be consistent with the observation that the dislocations are located closer to the interface in our study

than in the case of $PbTiO_3$ on $SrTiO_3$. It is also possible that differences in bond strength across the interface could account for a variation of the stand-off distance [25].

The unobserved stand-off distance in the current work may also be understood in terms of the extremely small critical thicknesses h_c for misfit dislocation formation. Theoretical considerations [2] have suggested that dislocation networks can only be formed once the film thickness exceeds a critical value, h_c. An implicit expression for h_c that includes the elastic anistropy is given by [3,26]

$$h_c = \frac{Kbd_f}{4\pi M\varepsilon_s d_s}\ln\left(\frac{\beta h_c}{b}\right), \tag{3}$$

with $\beta \approx 4$ [27]: dimensionless constant, $b \approx 0.3905$nm. M is the biaxial modulus for a cubic film with [100](001)film ‖ [100](001)substrate [3]

$$M = c_{11} + c_{12} - 2\frac{c_{12}^2}{c_{11}}, \tag{4}$$

(c_{ij} = elastic constants of the film) and K is the energy factor [26]:

$$K = (c_{11} + c_{12})\sqrt{\frac{c_{44}}{c_{11}}\frac{(c_{11} - c_{12})}{(c_{11} + c_{12} + 2c_{44})}}. \tag{5}$$

For $BaZrO_3$, theoretical values from first-principle calculations have been used ($c_{11} \approx 335$GPa, $c_{12} \approx 95$GPa, $c_{44} \approx 89$GPa [28]). As experimental elastic constants of the other film materials are not available, values for $SrTiO_3$ ($c_{11} \approx 315.6$ GPa, $c_{12} \approx 102.7$ GPa, $c_{44} \approx 121.5$ GPa [29]) have been used for $SrTi_{0.5}Zr_{0.5}O_3$ and $SrZrO_3$. In the case of the lowest mismatched system $SrTi_{0.5}Zr_{0.5}O_3$ / $SrTiO_3$, the critical

thickness is calculated to 1.6nm (≈ 4 unit cells), in the case of $SrZrO_3$ on $SrTiO_3$, the estimation yields 0.4nm (≈ 1 unit cell). For $BaZrO_3$ on $SrTiO_3$, the concept breaks down, namely, it is not possible to find a solution for equation (3) which implies a critical thickness in the order of one unit cell or less. This breakdown means that it is energetically favorable for misfit dislocations to be included in the heterogeneous nucleated epitaxial grains right from the beginning of growth. The estimation of the critical thicknesses, h_C, shows for all systems investigated, that the formation of misfit dislocations is energetically favorable right from the very initial stage of growth as the inital epitaxial grains consume other grains to convert the polycrystalline film into a single crystal.

General models for misfit dislocation formation in semiconductor thin films assume, that the dislocations nucleate at the film surface as loops and either glide or climb down towards the interface [30]. Because the glide plane of the dislocation array observed in our experiments is the interfacial plane (001), it is impossible for dislocations to glide from the surface to the interface in the current films. On the other hand, the dislocations could climb to the interface, but this is not consistent with current observations. Thus, for the current work, all evidence strongly suggests that the dislocations are included at the nucleation stage of epitaxy. These disclocations could nucleate at the edge of the initial epitaxial grains that nucleate at the interface during pyrolysis of the precursor. They could glide into the grain on the (001)-interfacial plane or climb from the edge to the interface. Heterogeneous nucleation of film grains is known to simultaneously occur at different sites along the interface, namely as island growth. During coalescence of epitaxial grains, a rearrangement of the dislocations, via glide, would be expected to equalize the distances between the misfit dislocations. It is concluded, that the slight residual stresses in the films ($d_\perp < d_p$ from XRD) are caused by an uncomplete rearrangement of misfit

dislocations, that could be influenced by defects of the $SrTiO_3$ surface, e.g. steps on the surface due to miscut. Although additional effects like phase transformation or thermal expansion mismatch on the lattice constant of the film can not be completely ruled out, they can not consistently explain the slight change in lattice constant.

5. CONCLUSIONS

Epitaxial films of cubic and pseudocubic perovskites with relatively high lattice mismatches can be grown on $SrTiO_3$ and $LaAlO_3$ substrates by the chemical solution deposition method. The epitaxy mechanism appeared to be the same as that discovered by Miller et al. [5] and described as epitaxial grain growth. The lattice mismatch was shown to be approximately fully accommodated by a network of interfacial misfit dislocations close to the interface along <100>-direction with Burgers-vector of <010>-type for lattice mismatches up to 7.4% ($BaZrO_3/SrTiO_3$). It was shown that the critical thicknesses for the formation of misfit dislocations are much too small to have a physical meaning for these highly mismatched perovskite systems. Therefore, it is hypothesized that misfit dislocations are introduced as the epitaxial grains, which are isolated from one another and located at the substrate/film interface, grow to consume all other grains as the polycyrstalline film is converted to a single crystal.

Acknowledgements

P. A. Langjahr would like to thank the "Deutscher Akademischer Austauschdienst" (DAAD) for a "DAAD-Doktorandenstipendium aus Mitteln des zweiten Hochschulsonderprogramms". F. F. Lange would like to thank the Alexander von Humboldt-Stiftung, whose award helped initiate the MPI/UCSB

interaction. We acknowledge support from AFOSR Contract F49620-94-1-0229 (re-charge for Langjahr at UCSB and support for Lange). This work also made use of the MRL Central Facilities supported by the National Science Foundation under award no. DMR-9123048.

REFERENCES

1. A.P. Sutton and R.W. Balluffi, *Interfaces in Crystalline Materials.*, Oxford University Press Inc., N.Y. (1995).

2. J.W. Matthews in *Epitaxial Growth, Part B* (edited by J.W. Matthews), Academic Press, N.Y. (1975).

3. W.D. Nix, *Metallurgical Transactions A* **20A**, 2217 (1989).

4. D.W. Pashley, in *Processing of metals and alloys* (ed. by R.W. Cahn), Materials Science and Technology, Vol. 15, VCH Verlag, Weinheim, Germany (1991).

5. K.T. Miller, C.J. Chan, M.G. Cain, and F.F. Lange, *J. Mater. Res.* **8**, 169 (1993).

6. Y. Dansheng, D. Yuandong, L. Rangjiao, W. Shiguang, *Chinese Journal of Low Temperature Physics* **15**, 410 (1993).

7. P.A. Langjahr et al., to be published.

8. S. Hoffmann, M. Klee and R. Waser, *Integrated Ferroelectrics* **10**, 151 (1995).

9. M. Pilleux, C.R. Grahmann, V.M. Fuenzalida and R.E. Avila, *Appl. Surf. Sci.* **65/66**, 283 (1993).

10. D. Taylor, *Br. Ceram. Trans. J.* **84**, 181 (1985).

11. JCPDS file, # 35-734 ($SrTiO_3$), #10-268 ($SrZrO_3$), #6-399 ($BaZrO_3$), #31-22 ($LaAlO_3$) (1992).

12. S. Geller and V.B. Bala, *Acta Cryst.* **9**, 1019 (1956).

13. F.F. Lange, *Science* **273**, 903 (1996).

14. P.A. Langjahr, T. Wagner, M. Rühle and F.F. Lange, *Mat. Res. Soc. Symp. Proc.* **401**, 109 (1996).

15. A.D. Polli, F.F. Lange, private communication (1995).

16. A. Strecker, U. Salzberger, J. Mayer, *Prakt. Metallogr.* **30**, 481 (1993).

17. B.D. Cullity, *Elements of x-ray diffraction* , Addison-Wesley Inc. (1978).

18. B.E. Warren, J. Biscoe, *J. Am. Ceram. Soc.* **21**, 49 (1938).

19. W. Bollmann, *Crystal Defects and Crystalline Interfaces*, Springer, Berlin (1970).

20. A. Recnik, P.A. Langjahr, P.D. Nellist, F. Ernst, S.J. Pennycook and M. Rühle, *Proc. 2nd Slovenian-German seminar on Joint Projects in Material Science and Technology*, (Schloß Ringberg, September 1996), pp. 28-29.

21. P.A. Langjahr, P.D. Nellist, et al., to be published.

22. S. Stemmer, S.K. Streiffer, F. Ernst, M. Rühle, *phys. stat. sol. (a)* **147**, 135 (1995).

23. V.V. Prisedsky, G.F. Pan'ko, V.V. Klimov, *Ferroelectrics* **64**, 257 (1985).

24. W. Mader and D. Knauss, *Acta metall. mater.* **40**, S207 (1992).

25. V. Vitek, G. Gutekunst, J. Mayer and M. Rühle, *Phil. Mag. A* 71, 1219 (1995).

26. A. J. E. Foreman, *Acta Met.* **3**, 322 (1955).

27 J. P. Hirth, J. Lothe, *Theory of Dislocations* , J. Wiley and Sons, N.Y. (1982).

28. R.D. King-Smith and D. Vanderbilt, *Phys. Rev. B* **49**, 5828 (1994).

29. Landolt-Börnstein, *New Series* , Springer, Berlin (1981).

30. L.B. Freund, *MRS Bulletin* **17**, 52 (1992).

TABLE CAPTIONS

Table 1: List of the systems investigated. Lattice constants d_f from literature and lattice mismatch strains ε_s between films and substrates $SrTiO_3$ ($d_s \approx 0.3905$nm) and $LaAlO_3$ ($d_s \approx 0.379$nm).

Table 2: Results of XRD-investigations of precursor powder heat treated at 1000°C/1h (Bragg-angles 2θ of the (002) reflections and calculated lattice constants d_p). The lattice constants of the powders d_p agree very well with values from literature (Table 1).

Table 3: Results of XRD-investigations of thin films heat treated at 1000°C/1h (Bragg-angles 2θ, full widths at half-maximum (fwhm) B and fwhm α of the rocking-curves of the (002) reflections of the films, calculated lattice constants $d_\perp$ and estimated sizes of the film grains D_f). $d_\perp$ is slightly smaller compared to d_p (see Table 2) for the films on $SrTiO_3$. The grain sizes of the epitaxial film grains D_f exceed the size of the grains in the powder suggesting that grain growth is enhanced in the films compared to the unoriented powder. All films show narrow fwhm α in rocking curves of the (002)-reflections of the films.

Table 4: Dislocation distances in $SrTi_{0.5}Zr_{0.5}O_3$-, $SrZrO_3$- and $BaZrO_3$-films on $SrTiO_3$ measured from n dislocation distances in HREM-micrographs (S_{HREM}, component in <010>-direction) and calculated from lattice constants determined by XRD (S_p) show good agreement, suggesting that the lattice mismatch strain is approximately fully relaxed by misfit dislcocations.

TABLES:

Table 1:

	$SrTi_{0.5}Zr_{0.5}O_3$ on $SrTiO_3$	$SrZrO_3$ on $SrTiO_3$	$BaZrO_3$ on $SrTiO_3$	$SrZrO_3$ on $LaAlO_3$
d_f (nm)	0.4003	0.4101	0.4193	0.4101
ε_s	0.025	0.05	0.074	0.082

Table 2:

	$SrTi_{0.5}Zr_{0.5}O_3$	$SrZrO_3$	$BaZrO_3$
2θ (°)	45.29	44.15	43.18
d_p (nm)	0.4005±0.0005	0.4103±0.0005	0.4190±0.0006

Table 3:

	$SrTi_{0.5}Zr_{0.5}O_3$ on $SrTiO_3$	$SrZrO_3$ on $SrTiO_3$	$BaZrO_3$ on $SrTiO_3$	$SrZrO_3$ on $LaAlO_3$
2θ (°)	45.42	44.29	43.35	44.18
$d_\perp$ (nm)	0.3994±0.0005	0.4090±0.0005	0.4175±0.0006	0.4100±0.0005
B (°)	0.4	0.28	0.24	0.26
D_f (nm)	22	32	39	36
α (°)	0.5	0.5	0.5	0.5

Table 4.

	n	S_{HREM} (nm)	S_p (nm)
$SrTi_{0.5}Zr_{0.5}O_3$	15	16.1 ± 5.4	15.6±0.8
$SrZrO_3$	45	7.5 ± 1.3	8.1±0.2
$BaZrO_3$	12	6.2 ± 1.0	5.7±0.1

FIGURE CAPTIONS

Fig. 1. SEM micrograph of the surface of a $SrTiO_3$-substrate. Steps can be identified, probably due to a miscut.

Fig. 2.Thermogravimetric analysis (TGA) of $SrZrO_3$- and $BaZrO_3$-precursors. The high weight loss is due to evaporation of solvent ($T \leq 100°C$) and pyrolysis ($T \leq 400°C$). During cooling, the weight is almost constant.

Fig. 3. X-ray powder diffraction of $SrTi_{0.5}Zr_{0.5}O_3$ - , $SrZrO_3$ - and $BaZrO_3$ - precursors heat treated at 1000°C/1h. All powders are of perovskite phase. In the case of $SrTi_{0.5}Zr_{0.5}O_3$, the reflections are broader and exhibit shoulders on both sides, indicating uncomplete mixing.

Fig. 4. X-ray (θ-2θ)-measurements of thin films of $SrTi_{0.5}Zr_{0.5}O_3$, $SrZrO_3$ and $BaZrO_3$ on $SrTiO_3$. The only orientation of the film detected by intense (002)-reflections is (001) film $\|$ (001) $SrTiO_3$. All other peaks are due to diffraction at the substrate (not only by CuK_α, but also by additional wavelengths within the x-ray source - like CuK_β and WL_α).

Fig. 5. An x-ray (θ-2θ)-measurement of a thin film of $SrZrO_3$ on $LaAlO_3$ also shows $(001)_f \| (001)_s$.

Fig. 6. X-ray texture analysis of the reflections a) (002) $SrZrO_3$ ($2\theta \approx 44.3°$), b) (110) $SrZrO_3$ ($2\theta \approx 30.9°$) and c) (110) $SrTiO_3$ ($2\theta \approx 32.4°$) shows the parallel orientation [100](001) $SrZrO_3$ $\|$ [100](001) $SrTiO_3$ of the $SrZrO_3$-film on the single crystal substrate.

Fig. 7. XRD pole figures of the (110)-reflections of a) a $BaZrO_3$-film on $SrTiO_3$ [(110) at $2\theta \approx 30.3°$] and b) a $SrZrO_3$-film on $LaAlO_3$ [(110) at $2\theta \approx 33.4°$].

Fig. 8. SEM-micrograph of a $SrZrO_3$-film on $SrTiO_3$. The film is relatively smooth.

Fig. 9. SEM-micrograph of a $SrZrO_3$ - film on $LaAlO_3$. The film consists of a network of connecting islands.

Fig 10. CTEM-micrograph of a cross-section sample of $SrZrO_3$ on $SrTiO_3$. The thickness of the film is approximately 45nm in the area shown.

Fig. 11. HREM- micrographs of $SrZrO_3$ on $SrTiO_3$ heat treated at 900°C/1h along a) <100>-zone axis and b) $<1\bar{1}0>$-zone axis. Burgers-circuits can be performed in both cases, leading to closure failues of a) $\mathbf{b} = d_S<010>$ and b) $\mathbf{b} = d_S/2<110>$. The distance between the extra half-planes observed is closer by a factor of $\sqrt{2}$ in case b) (for explanation, see Fig. 12).

Fig. 12. O-lattice model (unrelaxed) for two materials with simple cubic lattices (plan-view along [001]). Misfit dislocations are expected along the <100>-directions (wide lines). The inserted cross-sections along the <100>- and <110>-directions show that due to lattice mismatch, closure failures occur ($\mathbf{b} = d_S<010>$, resp. $\mathbf{b} = d_S/2<110>$). The separation distance along <110> [S (<110>)] is a factor of $\sqrt{2}$ smaller than along <100> [S (<100>)].

Fig. 13. HREM micrographs of a) $SrTi_{0.5}Zr_{0.5}O_3$, b) $SrZrO_3$ and c) $BaZrO_3$ on $SrTiO_3$ in <100>-zone axis in a lower magnification. Dislocations at the interface

are marked by arrows. As can be seen, the distance between the dislocations decreases with increasing lattice mismatch.

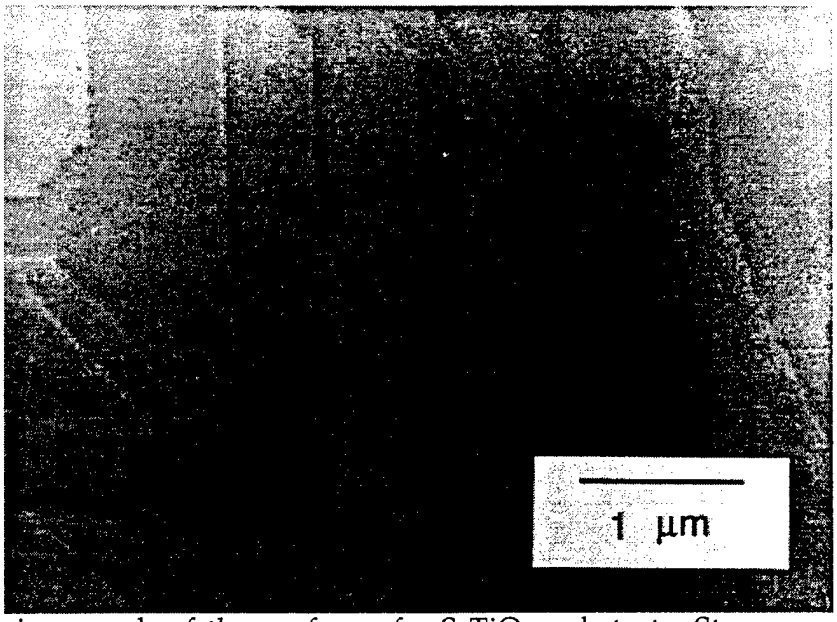

Fig. 1. SEM micrograph of the surface of a $SrTiO_3$-substrate. Steps can be identified, probably due to a miscut.

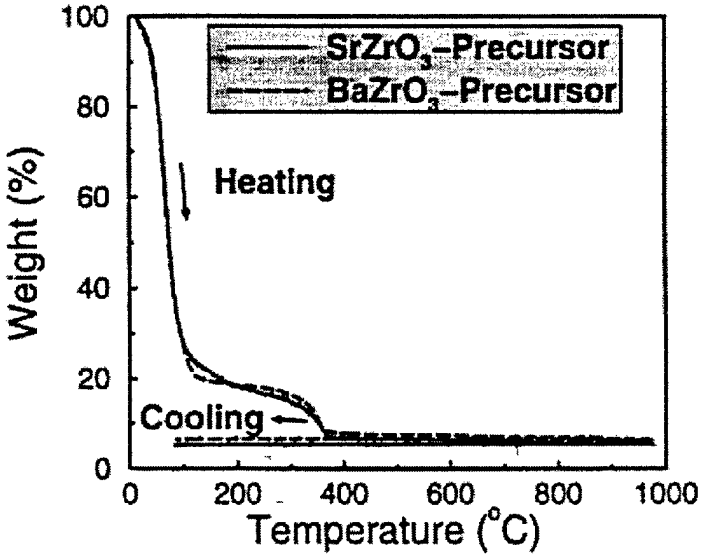

Fig. 2.Thermogravimetric analysis (TGA) of $SrZrO_3$- and $BaZrO_3$-precursors. The high weight loss is due to evaporation of solvent ($T \leq 100°C$) and pyrolysis ($T \leq 400°C$). During cooling, the weight is almost constant.

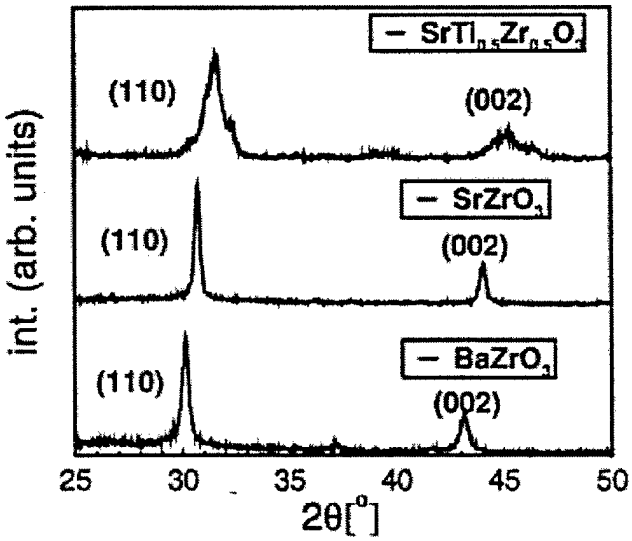

Fig. 3. X-ray powder diffractometry of $SrTi_{0.5}Zr_{0.5}O_3$ - , $SrZrO_3$ - and $BaZrO_3$ - precursor annealed at 1000°C/1h. All powders are of perovskite phase. In the case of $SrTi_{0.5}Zr_{0.5}O_3$, the reflections are broader and exhibit shoulders on both sides, indicating uncomplete mixing.

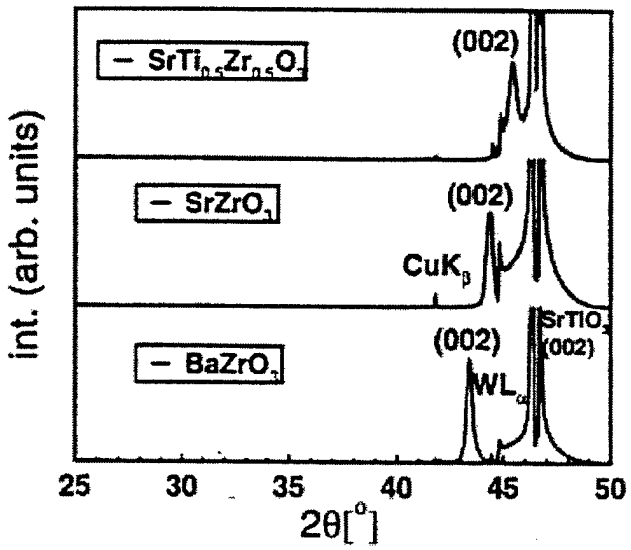

Fig. 4. X-ray (2θ/θ)-measurements of thin films of $SrTi_{0.5}Zr_{0.5}O_3$, $SrZrO_3$ and $BaZrO_3$ on $SrTiO_3$. The only orientation of the film detected by intense (002) reflections is (001) film | | (001) $SrTiO_3$. All other peaks are due to diffraction at the substrate (not only by $CuK\alpha$, but also by additional wavelengths within the x-ray source - like $CuK\beta$ and $WL\alpha$).

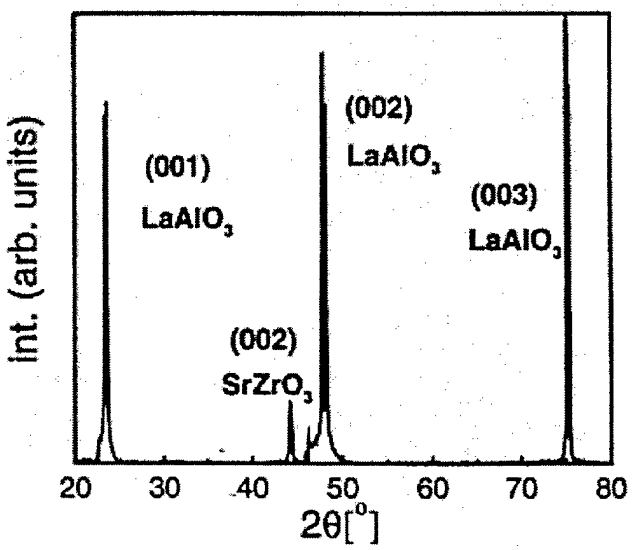

Fig. 5. X-ray (2θ/θ)-measurement of a thin film of $SrZrO_3$ on $LaAlO_3$ also shows (001)film | | (001)substrate.

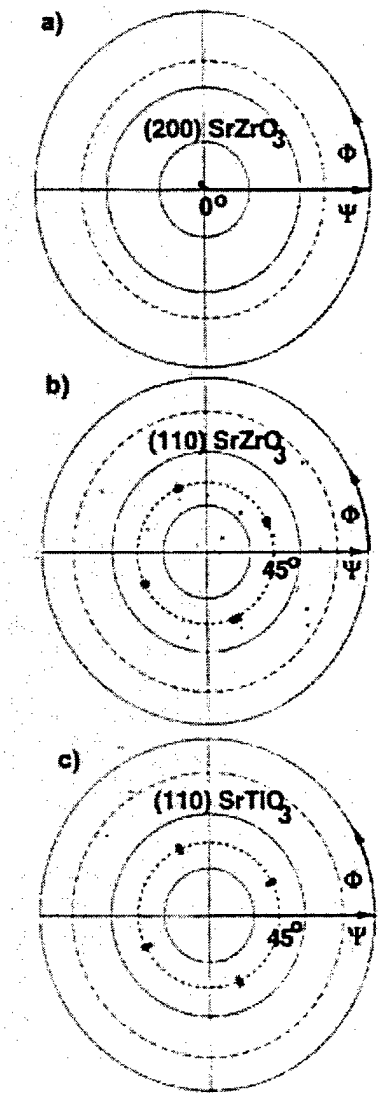

Fig. 6. X-ray texture analysis of the reflections a) (002) $SrZrO_3$ ($2\theta \approx 44.3°$), b) (110) $SrZrO_3$ ($2\theta \approx 30.9°$) and c) (110)$SrTiO_3$ ($2\theta \approx 32.4°$) show the parallel orientation [100](001) $SrZrO_3$ ❙❙ [100](001) $SrTiO_3$ of the $SrZrO_3$-film on the single crystal substrate.

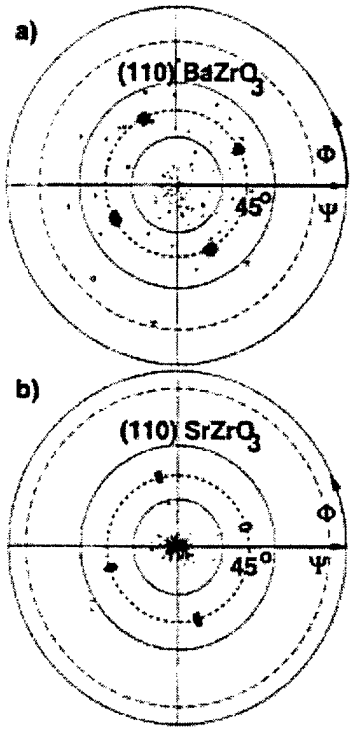

Fig. 7. XRD polefigures of the (110)-reflections of a) a $BaZrO_3$-film on $SrTiO_3$ [(110) at $2\theta \approx 30.3°$] and b) a $SrZrO_3$-film on $LaAlO_3$ [(110) at $2\theta \approx 33.4°$].

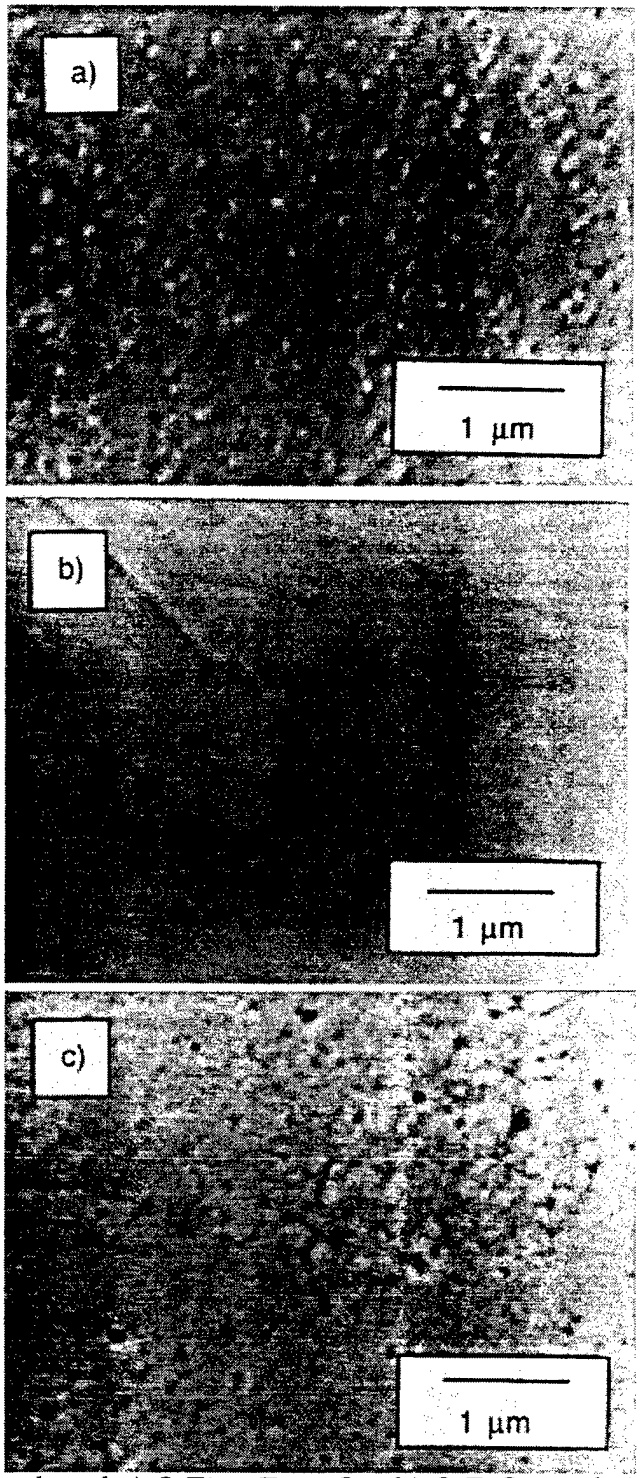

Fig. 8. SEM micrographs of a) $SrTi_{0.5}Zr_{0.5}O_3$, b) $SrZrO_3$ and c) $BaZrO_3$ on $SrTiO_3$. Relatively smooth films are obtained.

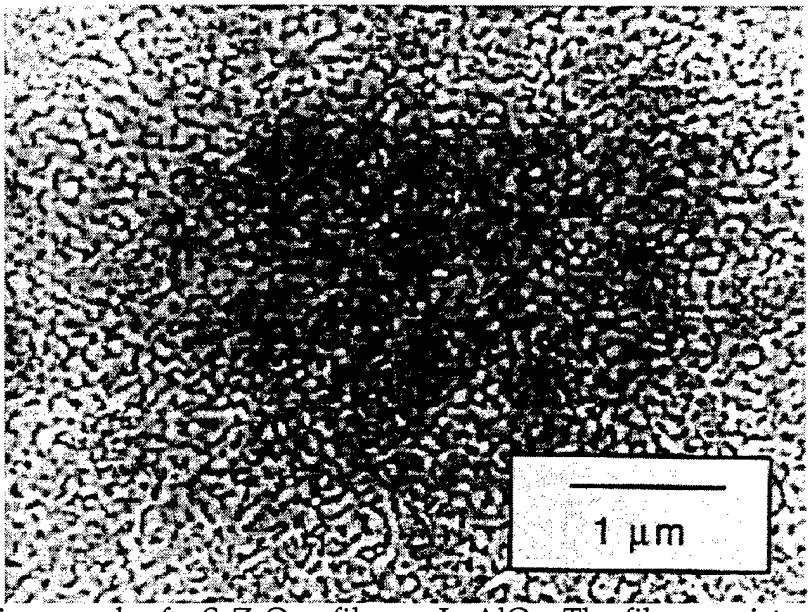

Fig. 9. SEM-micrograph of a $SrZrO_3$ - film on $LaAlO_3$. The film consists of a network of connecting islands.

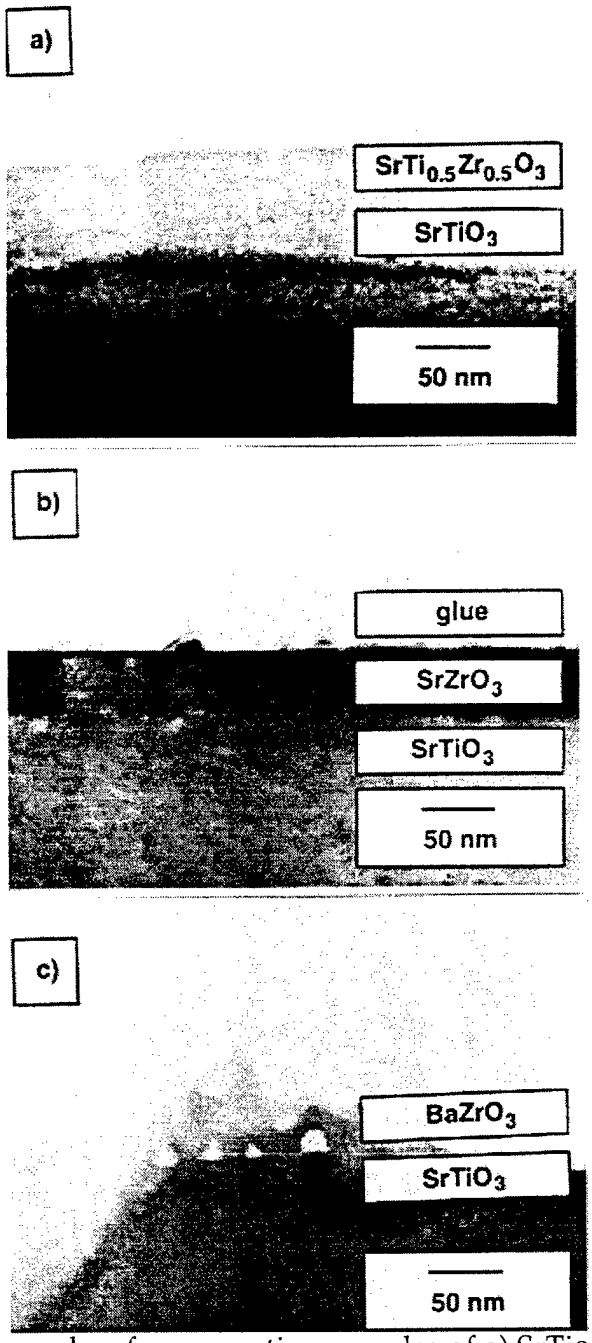

Fig 10. CTEM-micrographs of cross-section samples of a) $SrTi_{0.5}Zr_{0.5}O_3$, b) $SrZrO_3$

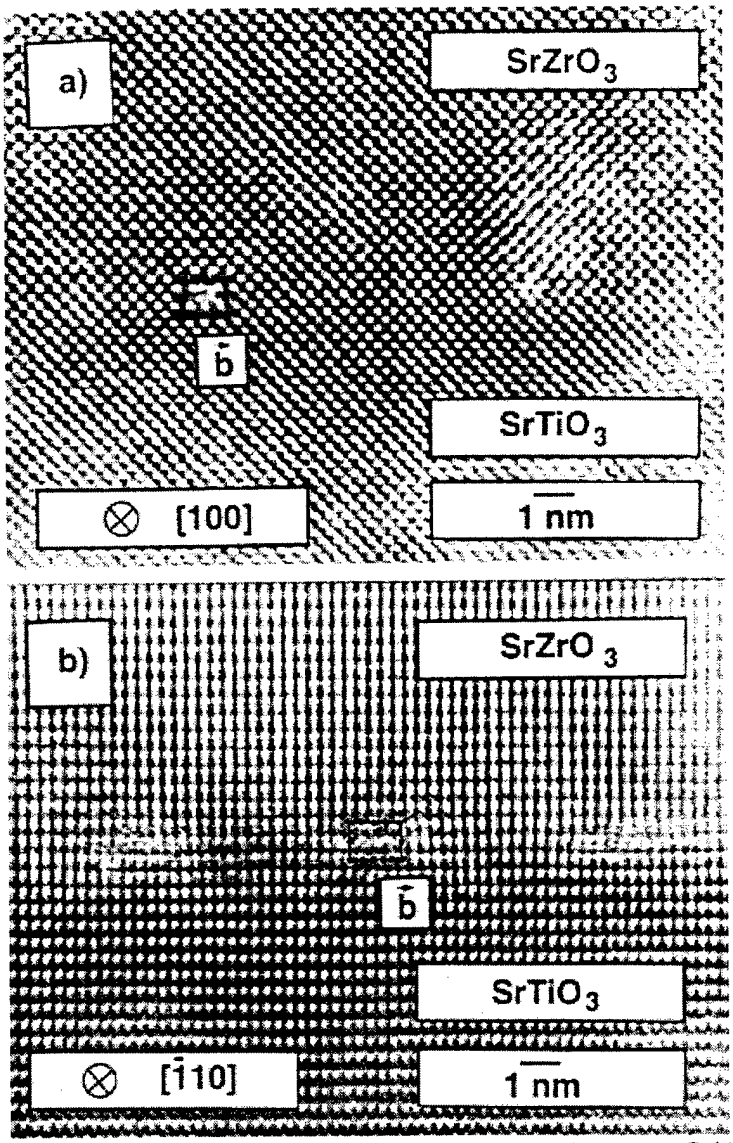

Fig. 11. HREM- micrograph of $SrZrO_3$ on $SrTiO_3$ annealed at 900°C/1h along a) <100>-zone axis and b) <11;$\bar{0}$>-zone axis. Burgers-circuits can be performed in both cases, leading to closure failues of a) **b** = a<100> and b) **b** = a/2<110>. The distance between the extra half-planes observed is closer by a factor of $\sqrt{2}$ in case b).

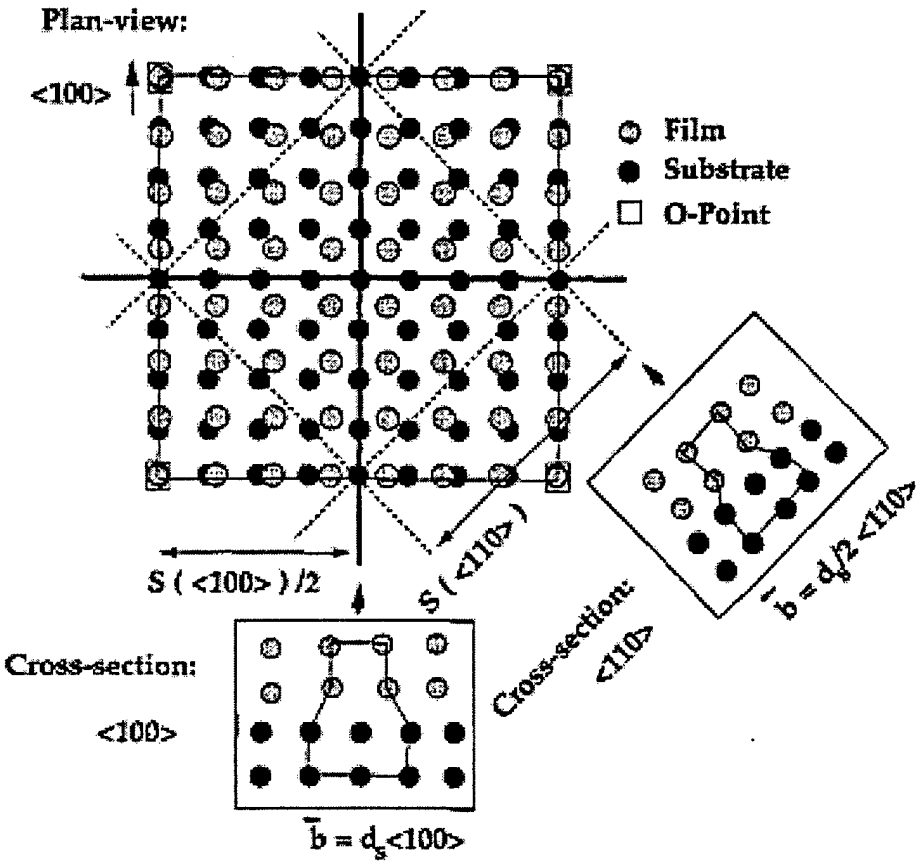

Fig. 12 O-lattice model (unrelaxed) for two materials with simple cubic lattices (plan-view along [001].

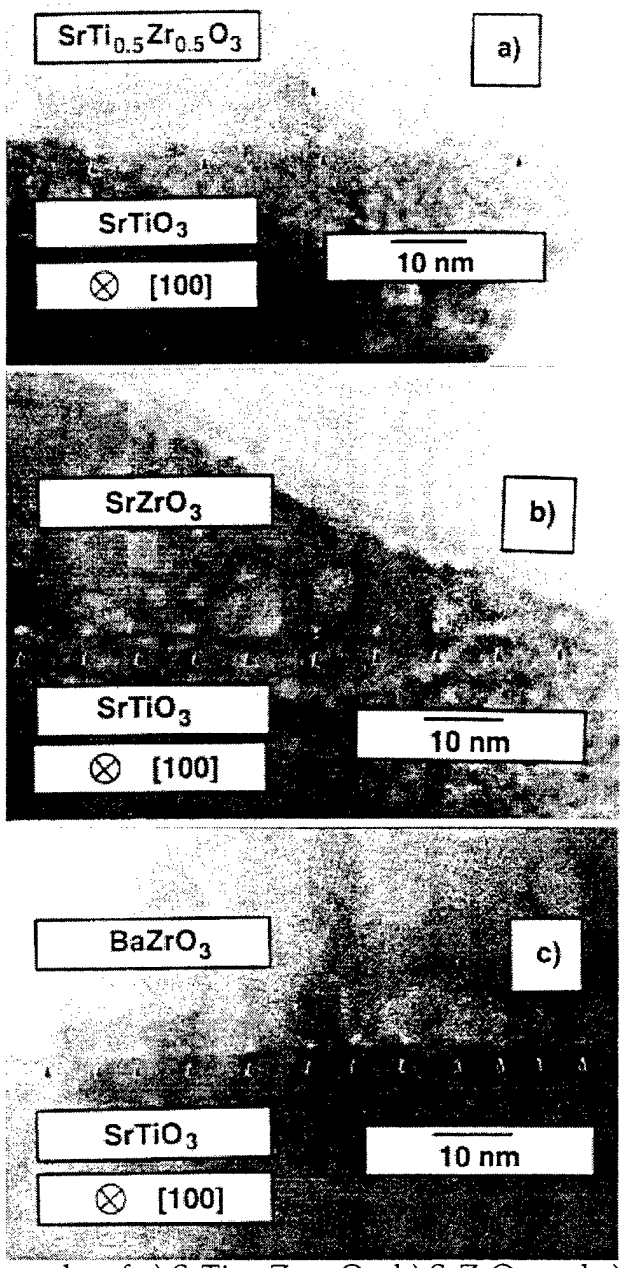

Fig. 13. HREM micrographs of a) $SrTi_{0.5}Zr_{0.5}O_3$, b) $SrZrO_3$ and c) $BaZrO_3$ on $SrTiO_3$ in <100>-zone axis in a lower magnification. Dislocations at the interface are marked by arrows. As can be seen, the distance between dislocations decreases with increasing lattice mismatch.